

A New Mechanism of Hook Formation during Continuous Casting of Ultra-Low-Carbon Steel Slabs

JOYDEEP SENGUPTA, BRIAN G. THOMAS, HO-JUNG SHIN, GO-GI LEE,
and SEON-HYO KIM

The initial stages of solidification near the meniscus during continuous casting of steel slabs involve many complex inter-related transient phenomena, which cause periodic oscillation marks (OMs), subsurface hooks, and related surface defects. This article presents a detailed mechanism for the formation of curved hooks and their associated OMs, based on a careful analysis of numerous specially etched samples from ultra-low-carbon steel slabs combined with previous measurements, observations, and theoretical modeling results. It is demonstrated that hooks form by solidification and dendritic growth at the liquid meniscus during the negative strip time. Oscillation marks form when molten steel overflows over the curved hook and solidifies by nucleation of undercooled liquid. The mechanism has been justified by its explanation of several plant observations, including the variability of hook and OM characteristics under different casting conditions, and the relationships with mold powder consumption and negative/positive strip times.

I. INTRODUCTION

OSCILLATION marks (OMs)^[1] and subsurface hooks^[2] in continuously cast steel slabs have received much attention from researchers during the past several decades, owing to their association with quality problems. Oscillation marks, such as shown in Figure 1(a), are periodic transverse depressions running across the slab surface. The nomenclature derives from their cause, vertical oscillation of the mold, although similar but irregular surface depressions occur even with a stationary mold.^[3] Oscillation marks form during the brief initial stage of solidification close (within ~ 15 mm) to the liquid steel level, where the solidifying shell tip meets the liquid meniscus. Indeed, variations in OM spacing are used to infer liquid level variations in the mold.^[4] Typically, OMs are 0.2 to 0.8 mm in depth, depending on steel composition and casting conditions.^[5] The spacing between OMs, called “pitch,” shown in Figure 1(a), ranges from 3 to 15 mm.^[5,6,7] Periodic oscillation of the mold facilitates uniform infiltration of the mold flux into the gap between the mold wall and steel shell, and is needed to prevent sticking and breakouts.

Subsurface “hooks” are distinctive microstructural features that accompany some OMs and can be identified by etching transverse sections through the slab surface.^[1,2,8] Figure 1(b) shows the 3-D shape of a typical hook beneath the root of an OM, which does not vary much with distance along the slab perimeter. Oscillation marks can be classified as “hook type” if they have a subsurface hook or “depression type” if they do not. Hooks can also be classified as “curved” if they angle steeply inwards from the surface or

“straight” if they are shallow and lie just beneath and parallel to the surface.^[9,10,11] Examples of each type of hook are shown in Figures 1(c) and (d). Oscillation marks associated with curved hooks are generally deeper and wider than those without any hooks or with straight hooks.^[12] Hooks often entrap mold flux, floating inclusions, and bubbles that ultimately form surface defects, such as slivers and blisters,^[13,14] after rolling and annealing. Furthermore, transverse cracks^[8,15,16] (included in Figure 1(a)) often initiate near the roots of OMs. This is due to the hotter, weaker shell and the associated coarser subsurface grain structure, and embrittling precipitates, caused by positive microsegregation (mainly of Al,^[8] Mn,^[8] N,^[8] and P^[16]) observed adjacent to hooks. In severe cases, the entire slab surface must be “scarfed” or ground to remove OMs, hooks, and their associated defects, leading to an overall loss of yield and productivity.^[9,17]

To minimize the defects associated with OMs and hooks, industry practice now tends to use higher oscillation frequencies and shorter strokes. This reduces the negative strip time (the period during each oscillation cycle when the mold moves downward faster than the casting speed) and produces shallower OMs.^[6,10,16] Practices to minimize the depth and severity of subsurface hooks include low density and exothermic mold powder,^[11] special submerged entry nozzles (SENs),^[12] nonsinusoidal or “triangular” mold oscillation,^[9,10] hot top molds,^[18] and replacing aluminum deoxidation with a silicon-killing practice.^[1] Steel grade greatly affects OM and hook formation. Oscillation marks are most severe in peritectic steels (0.07 to 0.15 pct C),^[19] while hooks increase in severity with decreasing carbon content, and especially plague ultra-low-carbon steels.^[7,20]

This work is part of a larger project to investigate the formation of OMs, hooks, and other phenomena related to initial solidification and surface defects in continuous-cast steel. This article first outlines and critically reviews previous theories of OM and hook formation. Then, a quantitative analysis of hooks and OMs is presented, based on numerous specially etched ultra-low-carbon slab samples obtained after controlled casting trials at POSCO Gwangyang Works. The remainder of the article presents a detailed

JOYDEEP SENGUPTA, formerly NSERC Canada Postdoctoral Fellow, is currently Research Associate with the Department of Mechanical and Industrial Engineering, University of Illinois at Urbana-Champaign, IL. BRIAN G. THOMAS, Wilkins Professor of Mechanical Engineering, is with the Department of Mechanical and Industrial Engineering, University of Illinois at Urbana-Champaign, IL. Contact e-mail: bgthomas@uiuc.edu HO-JUNG SHIN and GO-GI LEE, Graduate Students, and SEON-HYO KIM, Professor, are with the Department of Materials Science and Engineering, Pohang, University of Science and Technology (POSTECH), South Korea.

Manuscript submitted July 24, 2005.

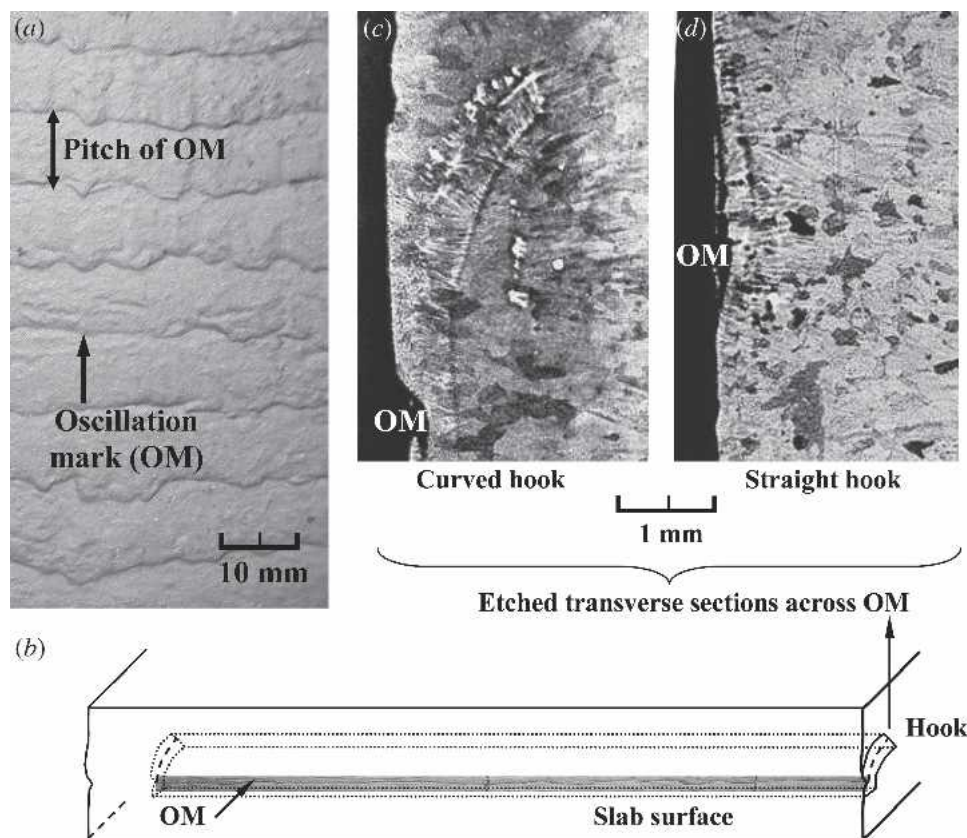


Fig. 1—OMs and hooks in an industrially cast ultra-low-carbon steel slab: (a) front-view: macrograph of surface; (b) 3-D schematic; (c) side-view: etched section of curved hook; and (d) straight hook.

mechanism for hook formation in ultra-low-carbon steel, which is also consistent with previous plant observations^[9,10] and with the results of previous theoretical modeling studies.

II. PHENOMENA INFLUENCING OM AND HOOK FORMATION

Understanding the formation of hooks, OMs, and other surface defects in continuous cast steel requires a proper consideration of the many distinct transient phenomena that occur simultaneously during the initial stages of solidification near the meniscus. Several of the most important of these interacting phenomena are summarized in Figure 2,^[21] and are described as follows:

- (1) *Change in meniscus shape due to fluid flow effects:* A dynamic balance between the surface tension, hydrostatic, and pressure forces at the three-phase junction, where the tip of the solidifying steel shell meets the liquid flux layer and the liquid steel creates a curved meniscus. At static equilibrium with no external pressure, the shape is given by Bikerman's equation.^[17] However, this shape can change during casting due to several different phenomena related to fluid flow. First, the vertical momentum of the steel jets entering the mold through the nozzle ports causes strong fluid flow, which can create standing waves across the mold width and perturb the free surface.^[22] Second, pressure forces from the oscillating mold^[8,23] can periodically alter the

meniscus curvature.^[24] Third, sudden metal level fluctuations may be caused by chaotic turbulent motion in the pool, buoyancy forces of floating argon bubbles, or by abrupt events, such as the release of a nozzle clog or gas pocket. These phenomena are important because the shape of the meniscus if it freezes^[25] ultimately determines the shape of final slab surface.

- (2) *Delivery of local superheat:* The superheat contained in the incoming liquid steel is transported across the mold by metal jets, which exit the nozzle ports and impinge on the solidification front. The superheat remaining in the liquid by the time it reaches the meniscus is typically about 30 pct of the original superheat temperature difference.^[26] This amount depends on the flow pattern in the liquid pool and varies with time, thus altering meniscus solidification.
- (3) *Heat transport between the solidifying shell and mold:* Liquid steel solidifies near the meniscus to form a solid shell according to the amount of heat conducted through the flux layers (both liquid and resolidified) and into the mold. This heat transfer is mainly governed by the size and properties of the interfacial gap near the meniscus.^[27] This in turn is affected by mold distortion, contact resistances, oscillating ferrostatic pressure, and strength of the newly formed shell. Thus, heat flux near the meniscus is highly nonuniform both in time and position.^[15] Recent measurements on ultra-low-carbon steel slabs^[5,28] using an experimental continuous casting simulator revealed that meniscus

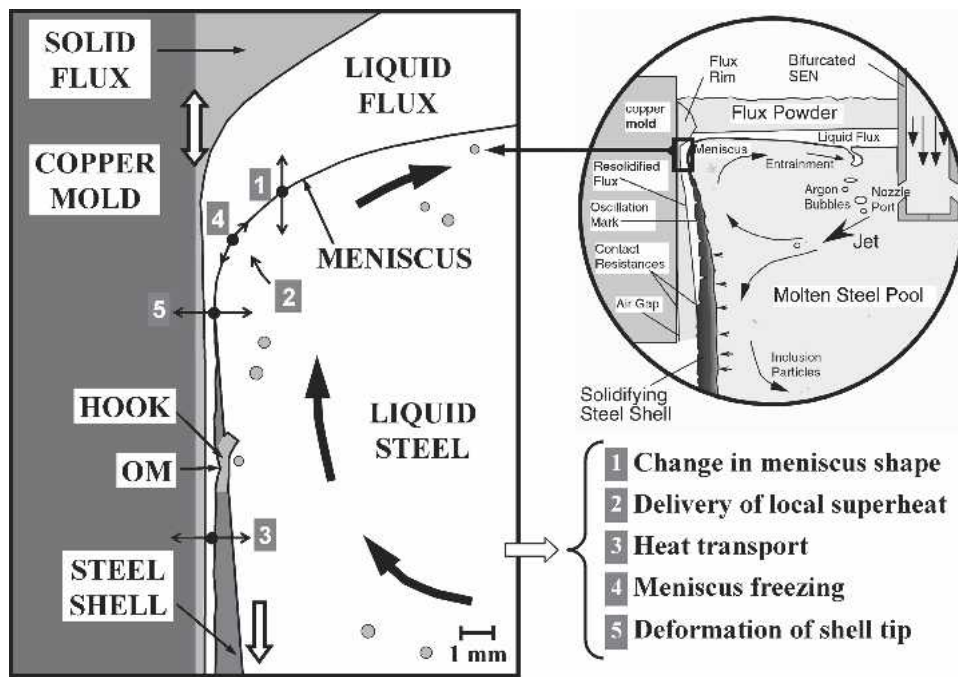


Fig. 2—Transient phenomena during initial solidification near the meniscus (left) inside a continuous caster mold^[21] (right).

heat flux rises rapidly during the negative strip time. This was attributed to latent heat released by meniscus freezing during this time.^[28]

- (4) *Meniscus freezing*: The high heat-transfer rates into a water-cooled mold can supercool the liquid and cause meniscus solidification far from the shell tip.^[18] Thus, the frozen instantaneous shape of the curved meniscus can be preserved in the final microstructure. Ultra-low-carbon steels are particularly prone to meniscus freezing, extending to ~10 mm from the mold wall, compared to ~3 mm in high-carbon steels.^[29] This was attributed to their higher liquidus temperature, thinner mushy zone (~15 °C freezing range vs ~50 °C for high carbon steels), and higher undercooling before nucleation (~200 °C vs ~145 °C for medium carbon steels).^[30]
- (5) *Deformation of the shell tip*: Heat transported from the steel shell to the mold changes if the solidifying shell tip distorts or bends away or toward the mold. The large transient temperature gradients in the shell tip may cause large stresses and distortion.^[31] This thermal distortion becomes more severe if the liquid level drops suddenly due to a flow fluctuation that momentarily exposes the interior shell surface to the molten mold flux.^[31] The amount of distortion also depends on the steel grade: a large shrinkage accompanies the $\delta \rightarrow \gamma$ transformation.^[30] The shell tip may bend away from the mold if the resolidified flux rim stuck to the mold wall that moves downward during the negative strip time increases the pressure in the liquid flux channel or pushes on the shell tip directly.^[1,8] Plastic deformation of the shell is also possible if part of the shell sticks to the mold walls, while the remainder is pulled downward at the casting speed.^[32] Shell tip distortion can evolve during the initial instants of solidification, changing the local heat flux and altering the final shape and size of surface defects on the slab.^[33]

III. PREVIOUS MECHANISMS FOR HOOK FORMATION

Several different mechanisms for OM and hooks have been proposed in previously published literature. They each account for one or more of the physical phenomena described in Section II, while ignoring others. Different combinations of events lead to different types of OM under different circumstances. For example, witness marks in the horizontal continuous casting^[34] and OM in the casting with oil lubrication^[32] form by different mechanisms than when casting with mold flux. The different mechanisms for hook formation proposed so far can be classified into three main groups.

- (1) *Discontinued shell growth-based mechanism*: Sticking to the mold wall during initial solidification disrupts shell growth. Subsequent solidification heals the disjointed shell edges, creating an OM.
- (2) *Shell bending and overflow-based mechanism*: The initial shell tip is forced to deform and bend away from the mold surface. Subsequent overflow of liquid steel over the curved shell surface creates a hook and OM.
- (3) *Meniscus solidification and overflow-based mechanism*: The curved meniscus solidifies. Subsequent overflow over this frozen meniscus forms the hook and its associated OM.

The first group of mechanisms^[32,35–38] focuses on events that disrupt growth at the shell tip. A gap between the new and the existing solidified shell has been proposed to occur in two different ways. First, according to Savage and Pritchard,^[36] the weak shell tip sticks to the mold surface and is torn off (brittle fracture due to low ductility at high temperatures) as the mold moves upward during the positive strip time. Alternatively, Sato^[35] and Szekeres^[32] have

suggested that the gap forms above the shell tip when liquid steel flows over it during the positive strip time and freezes against the mold wall. Subsequently, liquid steel flows into this gap, creating a “submeniscus.” During the negative strip time, this gap closes as the two solid edges weld together to create an OM. Events related to this mechanism are likely to occur during casting with oil, where the steel shell can directly contact and stick to the bare mold surface. However, this is less likely during casting with mold powder, where a stable flux layer between the steel shell and mold surface prevents direct shell-mold contact. Additionally, there is no evidence of hot tearing or welding in the micrographs presented in Figures 1(c) and (d). Thus, this mechanism was not the cause of hook-type OMs in ultra-low-carbon steel slabs, which are the subject of the current work.

The second group of mechanisms focuses on events that cause the tip of the solidifying shell to bend away from the mold wall. The causes of bending include the following: (1) viscoplastic deformation caused by thermal stresses,^[6] (2) changes in thermal-elastic-viscoplastic stresses caused by a sudden level drop,^[31] and (3) pushing on the shell by positive pressure in the liquid flux channel during negative strip.^[2] Subsequently, the meniscus overflows the deformed shell tip during the positive strip time and solidifies to create a depression, *i.e.*, an OM. If the deformed shell tip develops adequate strength and is not pushed back to the mold by the ferrostatic pressure, it will remain embedded in the solidifying material as a hook.

The uncoupled thermal-mechanical model of shell tip bending by Schwerdtfeger and Sha^[6] predicted inward tip bending up to ~ 0.6 mm, but the predicted OM depth did not decrease with higher mold oscillation frequencies and casting speeds, as observed in industry.^[39] The coupled thermal-stress model by Thomas and Zhu predicted a shell tip deflection of ~ 1.65 mm for a liquid level drop of 20 mm for 1.2 seconds, which occurs rarely. Recent work^[40] with this model predicts only 0.6-mm deflection for more common ± 10 -mm level fluctuations;^[41] hence, this mechanism alone cannot explain the deep hooks (up to ~ 2.5 mm) observed in every one of a series of OMs in an ultra-low-carbon steel slab.^[9] Finally, the bending theory of Emi *et al.*^[2] predicts that pressure buildup in the flux channel should push the shell *away* from the mold during the negative strip time. This is contradicted by the observation of *increased* heat flux during this time.^[28] Thus, thermal distortion mechanisms alone cannot explain OM formation in ultra-low-carbon steel.

The third group of mechanisms focuses on events that cause meniscus freezing^[1,18,29] during the negative strip time, coupled with deformation of the frozen meniscus^[12,14,42,43] due to the positive pressure in the liquid flux channel. These events are followed by overflow of liquid steel in the positive strip time to create the solidified hook. This general mechanism is consistent with the variability in hook curvature observed in a single sample, due to the time-dependent change of the meniscus shape caused by flow variations. In addition, higher flow velocities near the meniscus at the wide faces, predicted by many researchers,^[42,43,44] would increase the superheat supply and discourage meniscus freezing relative to the narrow face. This is consistent with the shallower hooks observed on the wide faces in industry.^[9,10,42,43] The meniscus freezing-based mechanism by Bo *et al.*^[12]

explains the decrease in hook depth with shorter negative strip time, higher casting speed, shorter stroke, and higher oscillation frequency. The positive microsegregation observed near the hook tip is explained by “sweating” (pumping out of segregated interdendritic liquid in the hook) due to the thermal expansion that accompanies reheating of the solidified meniscus when the hot molten steel overflows it.^[16]

These meniscus freezing-based mechanisms in previous literature are contradicted by the consistent rise in heat flow into the mold near the meniscus region observed only during each negative strip period, in experiments by Badri *et al.*, for ultra-low-carbon steel slabs.^[5,28] However, according to previous mechanisms, the overflow of liquid steel brings the meniscus closer to the mold during the *positive* strip time, which would *increase* heat flux during this period. Moreover, these mechanisms cannot explain the characteristic truncated shape of the curved hooks observed in Figure 1(c).

Based on this literature review, the formation of hook-type OMs appears to involve meniscus freezing. However, the detailed mechanisms need to be re-examined to include all of the phenomena and to match experimental observations. Toward this goal, the current study was conducted at the University of Illinois at Urbana-Champaign, focusing on ultra-low-carbon steels due to their greater propensity to form hook defects and their growing importance in the automotive industry.

IV. OBSERVATION OF CURVED HOOKS IN SLAB SAMPLES

Samples (100-mm long) from the narrow face of 230×1300 mm ultra-low-carbon steel slabs were obtained from plant experiments performed on a no. 2-1 slab caster at POSCO, Gwangyang Works (Gwangyang, South Korea), which features a conventional parallel-mold, standard two-port submerged entry nozzle, nonsinusoidal hydraulic

Table I. Conditions for Slab Cast at POSCO Gwangyang Works (Figures 8 through 14)

I. Steel Composition	
C(0.003 pct)-Mn(0.08 pct)-Si(0.005 pct)-P(0.015 pct)-S(0.01 pct)-Cr(0.01 pct)-Ni(0.01 pct)-Cu(0.01 pct)-Ti(0.05 pct)-Al(0.04 pct)	
II. Steel Properties	
Liquidus temperature (in °C)	1533
Solidus temperature (in °C)	1517
Density of liquid steel (in kg m ⁻³)	000
Surface tension at 1550 °C (in N m ⁻¹)	.6
III. Slag Properties	
Solidification temperature (in °C)	1101
Melting temperature (in °C)	1145
Viscosity at 1300 °C (in Poise)	2.62
IV. Casting conditions	
Casting speed	23.23 mm s ⁻¹ (1.394 m min ⁻¹)
Frequency of mold oscillation	2.90 Hz (174 cpm)
Stroke of mold oscillation	5.89 mm
Theoretical pitch (speed/frequency)	8.01 mm
Superheat	32 °C

oscillator, and electromagnetic breaking. The composition and typical casting conditions are given in Table I. Further details on these industrial trials are given elsewhere.^[9,10] Sections through each narrow face sample were cut, polished, and etched with a special picric acid solution to reveal the “primary” microstructure, including the dendrites, grain boundaries, hooks, and OM that formed during initial solidification. These microstructures differ greatly from the final grain structures revealed by traditional nital etching after many subsequent phase transformations.^[1,8,16]

Figure 3(a) shows a curved hook and its associated OM in a typical sample. Each hook has a curved line along its center, determined to be the line of hook origin that reveals the shape of the meniscus after freezing. Dendrites grew away from this line in both directions. Those growing toward the molten steel indicate the thickness of the solidifying hook prior to a sudden change in conditions. Those growing toward the mold wall likely occurred after the frozen meniscus surface was overflowed with new liquid steel. In Figure 3(a), the hook depth, D , is the perpendicular distance from the slab surface to the furthest inner extent of the hook and indicates the thickness of the surface layer that has to be removed to eliminate the hook. The hook extends from its starting point (O), along the line of hook origin, to its end point (E). The hook shell thickness, T , generally represents the thickest part of the hook.

A. Metallographic Assessment of Hook Shapes

Figures 3(b) and (c) compare the lines of hook origin (dotted lines) of successive hooks observed on two ~100-mm-long slab samples, cast under different conditions. The wide variation of hook depth and shape indicates that hook formation is a complex event dictated by instantaneous meniscus shape when it freezes. Thus, the events during initial solidification (Section II) alter the curvature of the molten steel balanced on the shell tip.

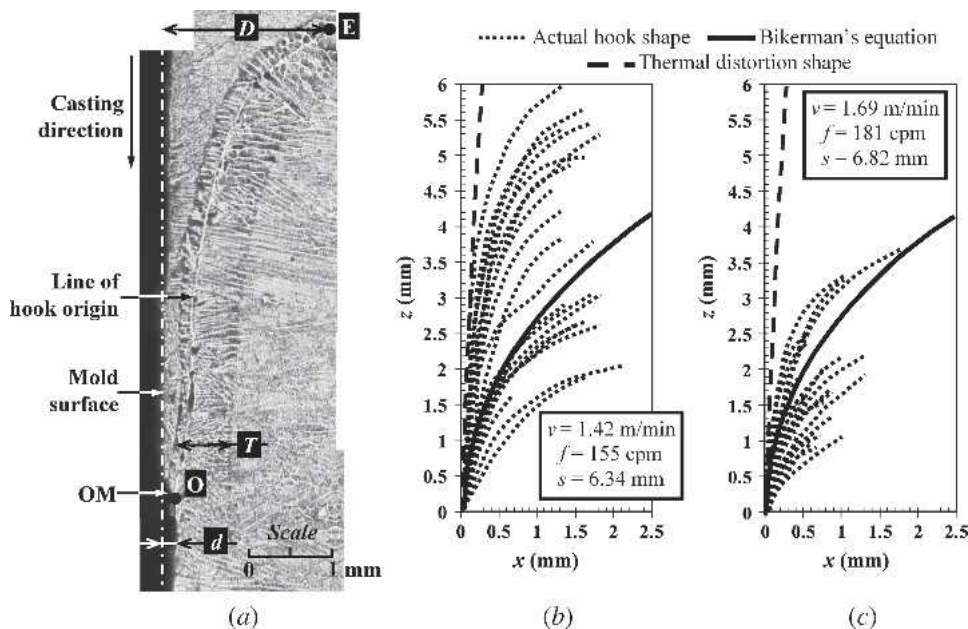


Fig. 3—(a) Typical curved hook and OM in ultra-low carbon steel slab, and (b) and (c) line of origin of successive hooks on slab samples cast under two different conditions. Comparison with Bikerman's equation and predicted shell shape after a level fluctuation is also included.

Traces of bubbles, entrapped mold powder, and inclusions were often observed near curved hooks, as shown in Figures 4(a) through (c). Bubbles (Figure 4(a)) and debris (Figure 4(b)) can be present on both sides of the line of hook origin. From below the frozen meniscus, particles flow up with the steel and are trapped by the meniscus before they can enter the slag layer (“A” in Figure 4(a)). From above the frozen meniscus, particles flow along with the overflowing liquid steel, roll down the curved meniscus, and are entrapped near the slab surface (“B” in Figure 4(a)). Large particles floating over the frozen meniscus can disrupt the overflow, creating additional surface depressions near the OM, as shown in Figure 4(c).

The meniscus shape on the shell tip before freezing and after overflow dictates the OM depth, hook depth, and angle. In Figure 5(a), a shallow OM and hook are found when the meniscus shape is almost straight and the overflow region has a shallow contact angle. In contrast, the deeper OM in Figure 5(b) has a near-vertical contact angle in the overflow region. This was perhaps facilitated by the formation of a deeper hook with larger curvature. Strange shapes of the hook and overflow region produce irregular surface depressions, as shown in Figure 5(c).

Three different hooks from the same slab sample shown in Figures 6(a) through (c) provide evidence that the hook tip can separate from the solidified shell. The separation appears to be caused by brittle fracture due to inertial and buoyancy forces (ignored in the previous analyses) acting on the tip when molten steel overflows the curved hook. The edges of the hook tip and the fractured hook in Figure 6(a) align almost exactly, except for a small portion of the left edge that was apparently melted away by the incoming liquid steel. The rest of the hook tip remained entrapped in the solidifying shell growing above the hook. The fractured shell tip in Figure 6(b) was carried by the overflowing liquid to the slab surface. Similar events explain the truncated end observed in almost all hooks, such as in Figure 6(c).

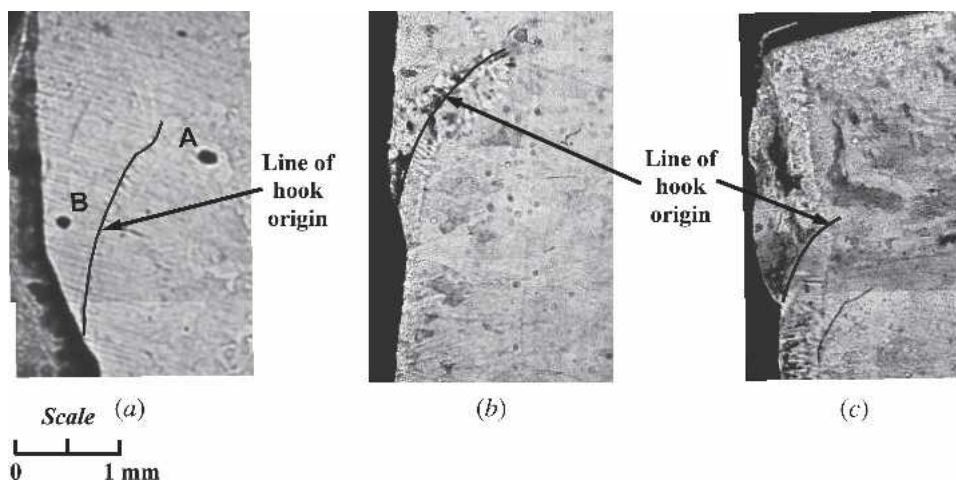


Fig. 4—Locations of (a) bubble, and (b) and (c) inclusion debris entrapped near the line of hook origin in three cast samples.

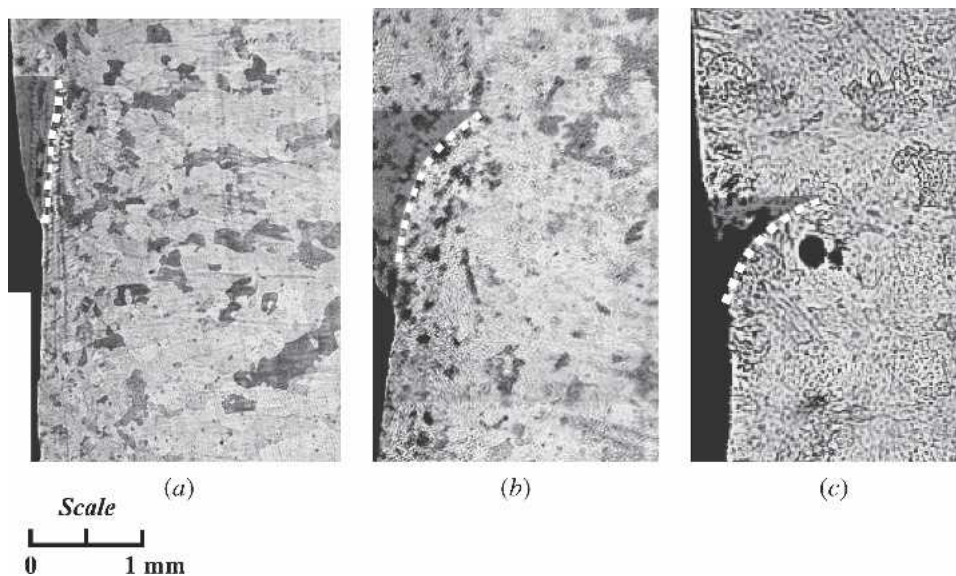


Fig. 5—Etched samples showing different shapes of frozen meniscus (dotted line): (a) almost straight to (c) very curved; and different shapes of overflow region (shaded): (a) shallow contact angle, (b) near-vertical contact angle, and (c) strange angle and shape.

The etched hook sample in Figure 7 clearly reveals dendrites originating from several different nucleation sites located on or near the frozen meniscus (*i.e.*, line of hook origin). Solidification proceeded in both directions, as evidenced by increasing interdendritic segregation and coarsening with distance from this line. Some dendrites grew away from the mold wall. Others grew into the liquid overflow region toward the mold wall, stopped growing, and coarsened, as temperature gradients dropped. The rest of the overflowed region solidified outward from the mold wall, producing a finer structure, as heat was rapidly removed by the mold. A group of dendrites growing toward the molten steel abruptly changed direction near the truncated edge, in contrast to the uninterrupted growth in the same direction nearer to the base of the hook. This suggests that the truncated hook tip moved during the overflow.

B. Hook Shape Variation with Plant Conditions

Shin *et al.*^[9,10] quantified the effect of casting speed, oscillation conditions, and superheat on mold powder con-

sumption rate, OM depth, and hook characteristics, based on analysis of data and slab samples obtained in controlled plant trials. The mold powder consumption rate per oscillation cycle was found to increase with increasing both positive strip time and negative strip time. Increasing superheat greatly decreases hook size, including both length and depth. Higher oscillation frequency shortened the hook and decreased the angle of thick hooks. Hook depth increased with increasing negative and positive strip time and was directly proportional to hook shell thickness. Finally, shorter shallower hooks correlated slightly with shallower OMs. Further details are published elsewhere.^[9,10]

V. METHODOLOGY

The phenomena described in Section II show that the formation of OMs and hooks involves complex, interdependent, and transient events. The microstructures and plant observations in Section IV provide important new information, but cannot reveal the detailed steps that lead to the

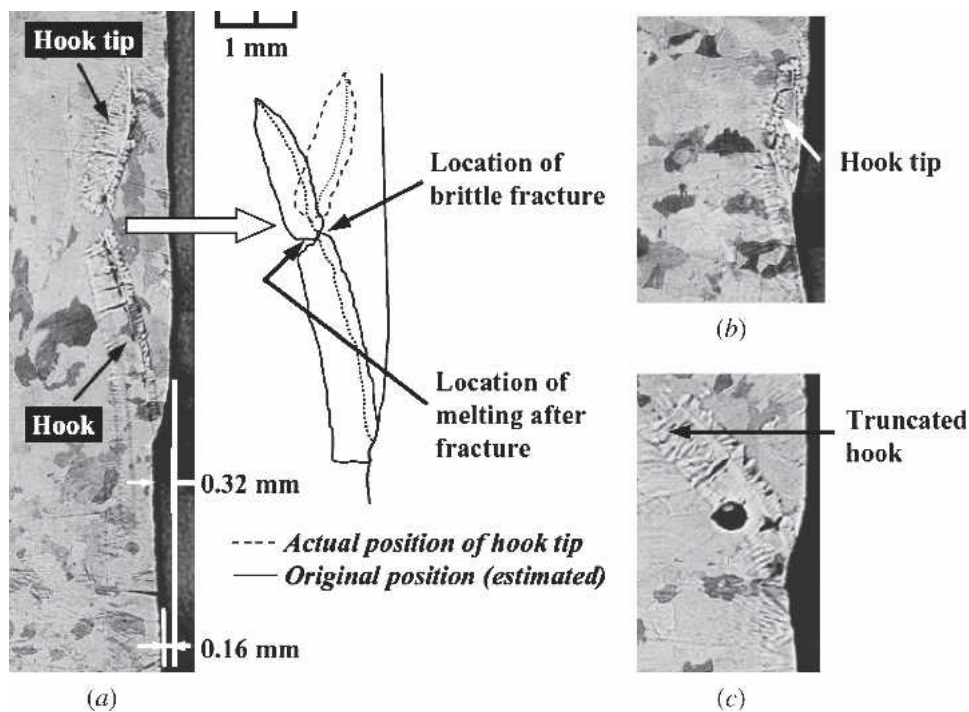


Fig. 6—Three hooks showing (a) evidence of brittle fracture of hook tip, which (b) floated to the slab surface or melted/drifted away, leaving (c) characteristic truncated hook.

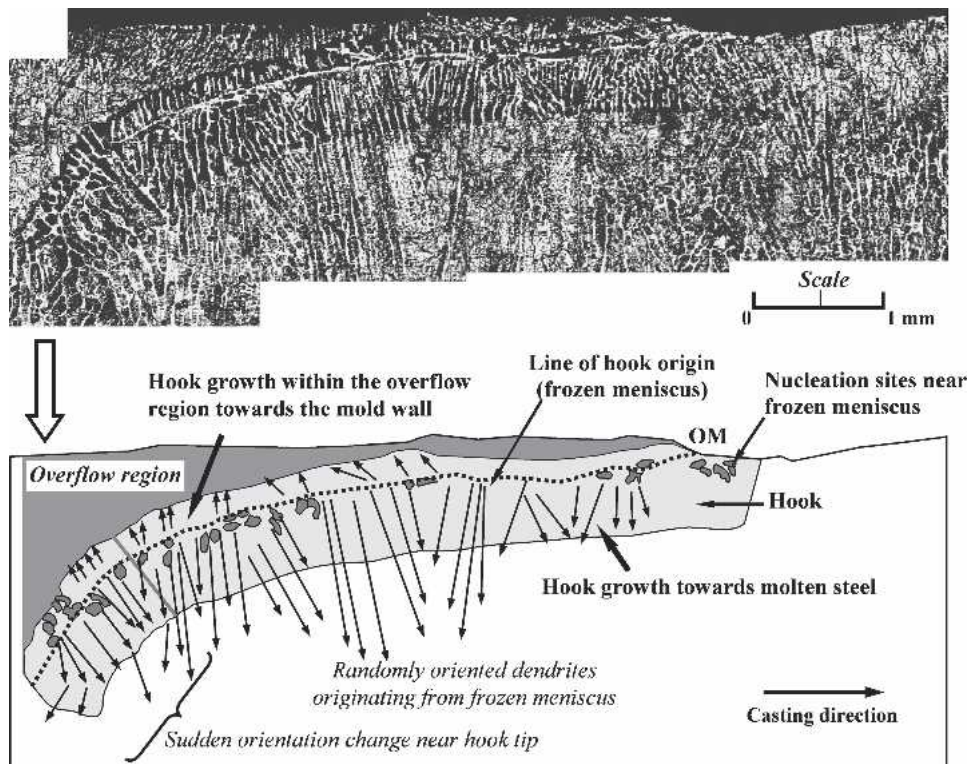


Fig. 7—Hook micrograph showing directional growth of dendrites from the line of hook origin (frozen meniscus).

final microstructure and morphology. Developing a comprehensive mathematical model to predict these events is a daunting task, requiring fully coupled, transient thermal, fluid-flow, and stress analysis. Hence, an alternative methodology is adopted in this work: to combine existing mod-

eling results and plant observations together to construct a series of schematics that illustrate the behavior as accurately as possible. These schematics might not be quantitative, but they clearly explain the detailed mechanism of hook and OM formation.

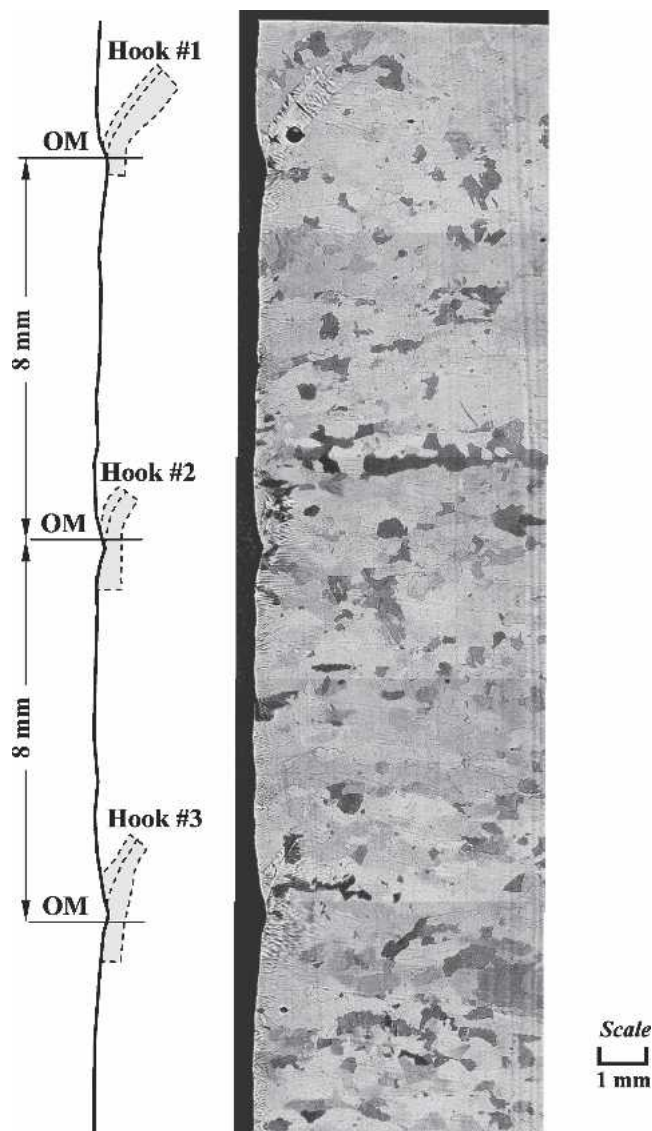


Fig. 8—Three consecutive hook-type OMs in an ultra-low-carbon steel slab (Table I). Solid and dotted lines (left) outline the slab surface and hook shapes and are used in Figure 10.

In this study, the time-dependent positions of the mold, slag rim, solidifying shell, and meniscus are graphically tracked to explain the occurrence of OM 1 in Figure 8. This figure shows three consecutive hook-type OMs (separated by the theoretical pitch of 8 mm) observed on an ultra-low-carbon steel slab cast with a casting speed of 23.23 mm s^{-1} , an oscillation frequency of 2.90 Hz, and a stroke length of 5.89 mm. The variation of mold and shell velocity with time and the negative strip period for this case are shown in Figure 9(a). The temporal variation in positions of the mold and OM 2 relative to the far-field meniscus (*i.e.*, laboratory frame of reference) is shown in Figure 9(b). The first frame (time, $t = 0$ in Figure 9(b)) was created by systematically plotting the positions of the mold, meniscus, slag rim, solid shell, flux channel, hooks, and OMs 2 and 3 on a x - z Cartesian space, with x direction representing distance through the slab thickness and z direction representing vertical distance along the slab length. The $x = 0$ line is the mold surface. The $z = 0$ line indicates the mold position

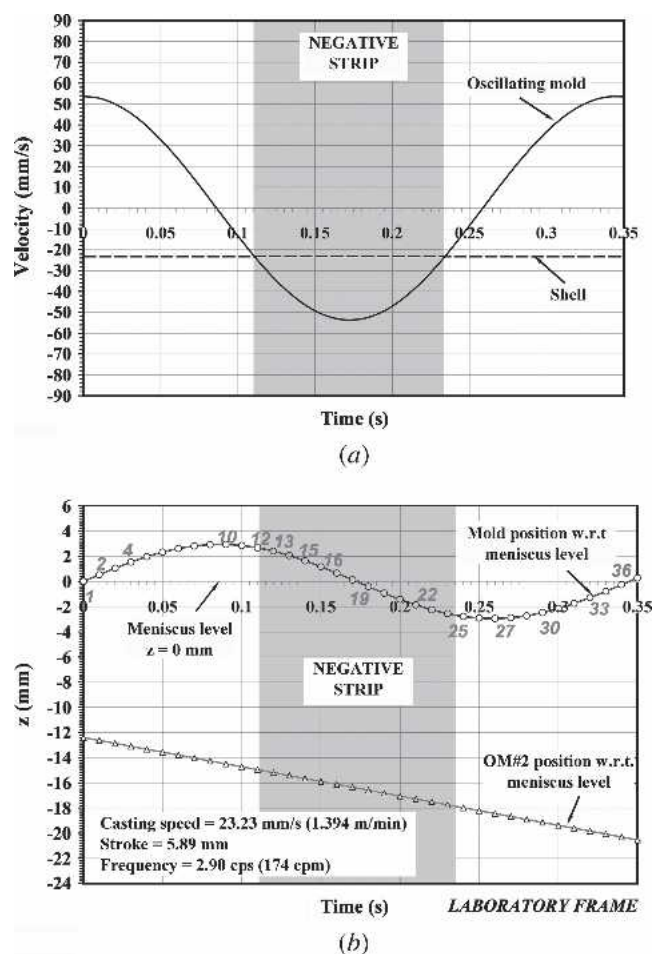


Fig. 9—Histories of mold and shell (a) velocity and (b) position relative to the far-field meniscus (laboratory frame) for conditions in Table I. Numbers indicate frames in Figures 10 and 13.

midway between oscillations and at time $t = 0$, coinciding with the far-field metal level in the mold, which is assumed to remain unperturbed at all times.

The initial frame in the sequence is enlarged in Figure 10. At $t = 0$, the mold acceleration is zero, as its mean position ($z = 0$) matches the far-field metal level. Hence, the mold will not exert any inertia forces on the meniscus *via* the liquid flux channel. Also, the positive pressure generated in the flux channel during the negative strip time from the previous cycle is assumed to be completely released by the time the mold reaches the start of next cycle. Thus, in the absence of surface waves, the initial shape of the meniscus is the equilibrium shape, determined by the balance of surface tension and ferrostatic pressure forces given by Bikerman's equation.^[17,45] The surface tension depends greatly on the sulfur content in the steel being cast^[46] and slightly alters the meniscus shape, as given by the Bikerman's equation, plotted in Figure 11. Corresponding to the sulfur content of 0.01 pct (Table I) for the ultra-low-carbon steel slab, a surface tension of 1.6 N m^{-1} was chosen. The steel density was assumed to be 7000 kg m^{-3} at $1560 \text{ }^{\circ}\text{C}$ ^[45] (tundish temperature was $\sim 1566 \text{ }^{\circ}\text{C}$).

The position of the solid flux rim was extrapolated from the contour at the flux solidification temperature in the temperature distribution computed by Takeuchi *et al.*^[23]

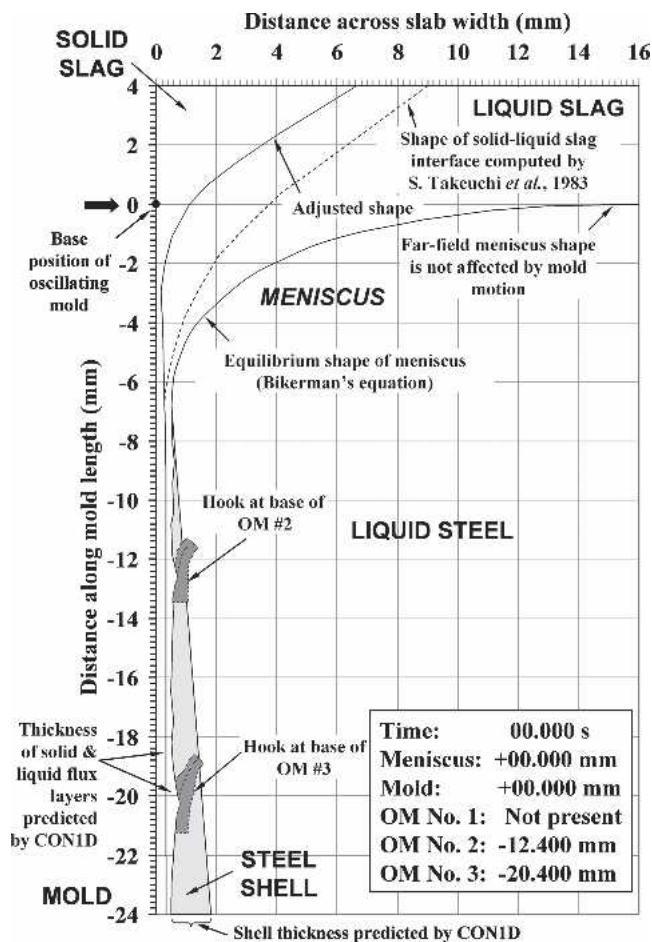


Fig. 10—Positions of the meniscus, solid shell, hooks, OM, slag rim, and mold (black arrow) at time $t = 0$ s (frame 1).

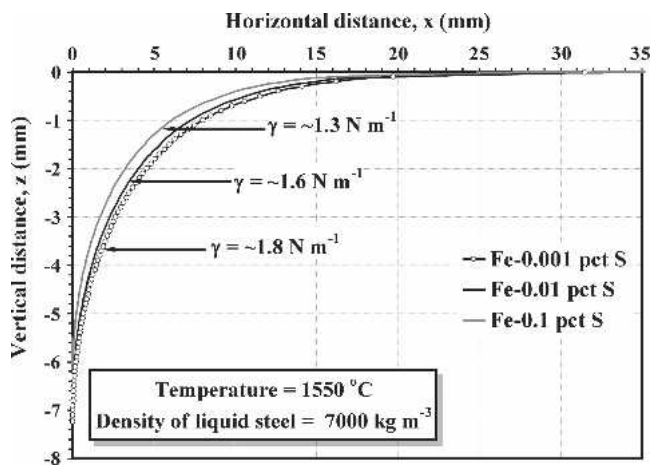


Fig. 11—Effect of sulfur content on surface tension^[45] and meniscus shape (Bikerman equation^[44]).

Taking into account the higher flux melting temperature (1130 °C^[23] vs 1145 °C^[10]) and higher superheat (20 °C^[23] vs 32 °C^[10]) in this work, the solid flux rim position was adjusted to be higher in constructing Figure 10.

To construct Figure 10 ($t = 0$), a one-dimensional finite-difference solidification model of the shell and interfacial gap, CON1D,^[27] was applied for the conditions of the plant

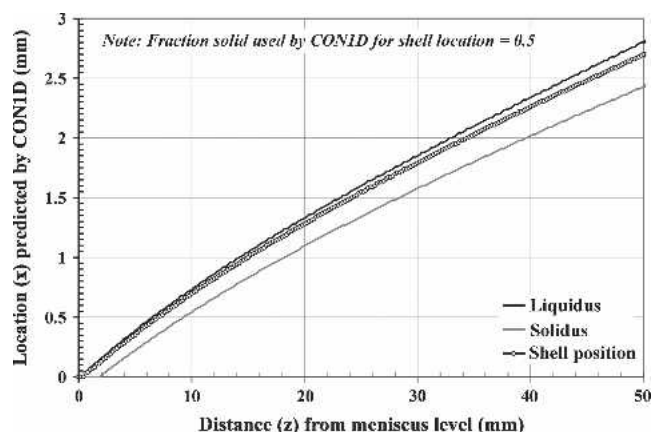


Fig. 12—Thickness profile of solid shell predicted by CON1D^[26] (Table I conditions), used in Figure 10.

trial (Table I). The computed thicknesses of the liquid and resolidified flux layers (0.22 and 0.34 mm) were used in constructing the “results” figures. The computed thickness profile of the steel shell along the mold was also used, as shown in Figure 12. The shell thickness at the bottom of the figure (~ 18 mm below the shell tip) is ~ 1.3 mm. The profile of the left edge of the slab, hook, and OM shapes was traced from Figure 8.

Events that form OM 1 start as the mold travels upward from its mean position (frame 1). Each subsequent figure was constructed by altering the preceding figure using logical scientific principles, including the following constraints. (1) The mold position was taken from Figure 9(b). The solid flux rim was assumed to be perfectly attached to the mold wall and oscillated accordingly. The OM and hooks move down with the solid shell at the casting speed. The shell thickness profile stays constant with time, except at the shell tip and opposite the hooks. (2) The meniscus shape changes due to pressure changes during the positive and negative strip periods. Dynamic changes of the meniscus shape during an oscillation cycle were observed by Tanaka and Takatani,^[24] on a silicon oil-water interface inside an oscillating acrylic mold. The meniscus flattens due to the positive pressure in the flux channel during the negative strip time and bulges outward due to the negative pressure in the flux channel during the positive strip time. Similar effects have been predicted by fluid flow models.^[47] Thus, movement of the solid flux rim was assumed to vary the flux pressure and distort the meniscus appropriately. The instantaneous shape of the meniscus becomes the line of hook origin for OM 1 when it freezes. Solidification from this line then evolves into the hook shell thickness. As the shell moves downward, OM 1 and its hook form and grow, while OM 3 gradually moves out of the frame. (3) For each frame in Figure 9(b), the meniscus never touches the mold, the contact angle of liquid steel overflowing the frozen steel surface stays constant, solidification logically proceeds only from cold to hot regions, and melting occurs with heat input as appropriate.

With this methodology, 36 frames were created in MICROSOFT POWERPOINT* 2003, completing one full

*MICROSOFT POWERPOINT is a trademark of Microsoft Corporation.

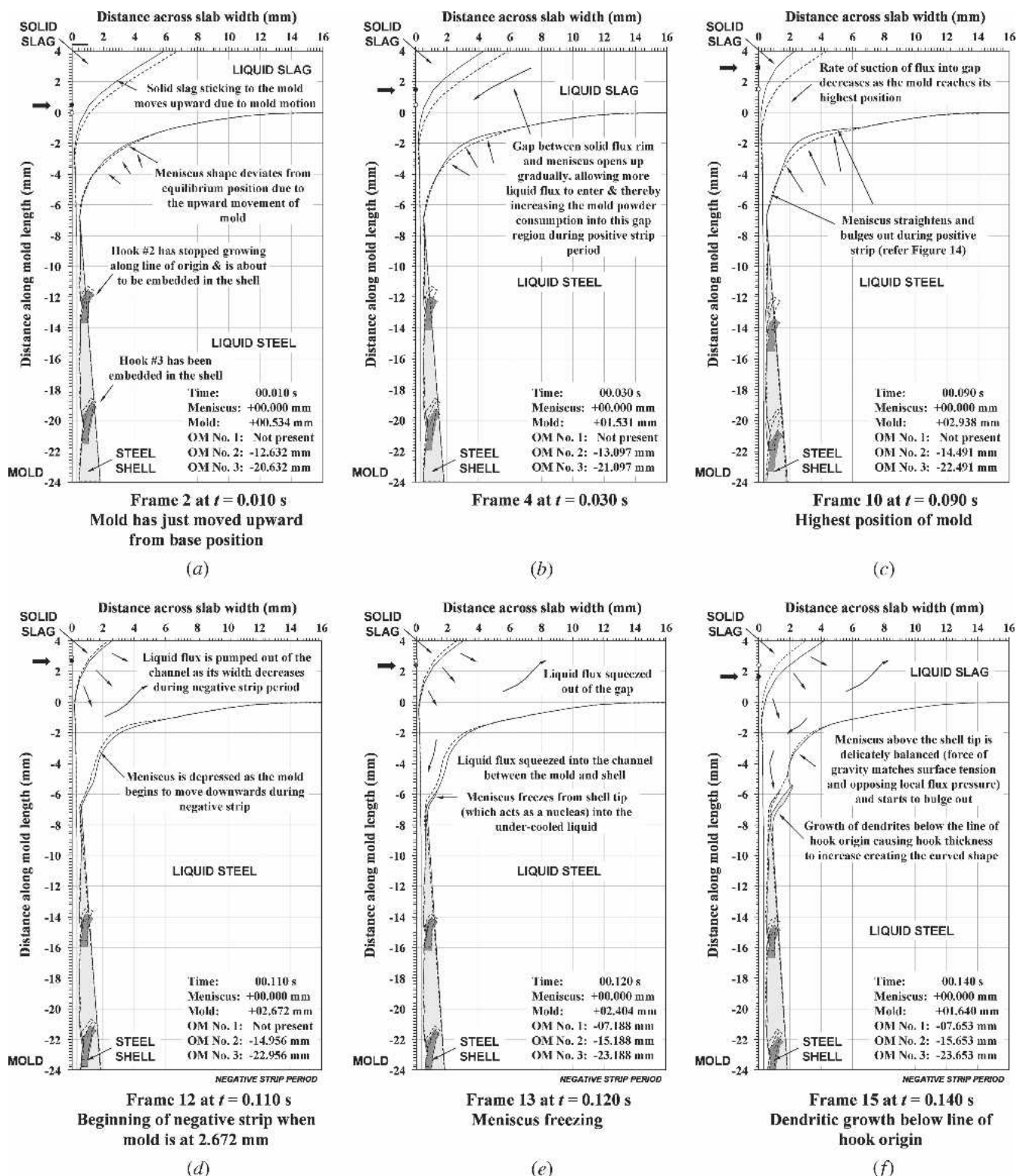
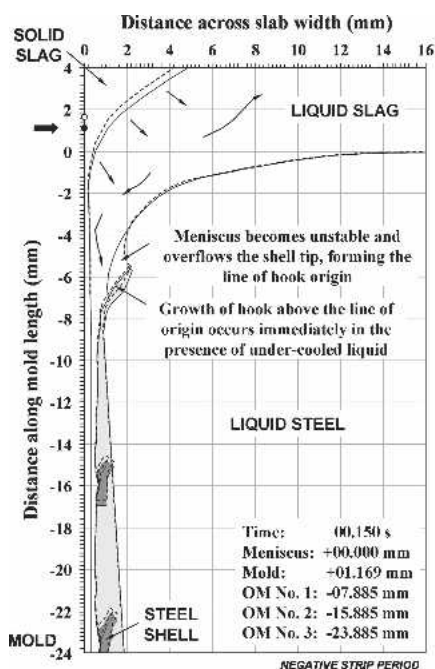


Fig. 13—(a) through (n) Frames depicting events in hook formation, compared with (o) actual slab sample (Table I conditions). Dotted lines indicate positions in the preceding frame.

oscillation cycle in steps of 0.01 seconds for a total time of 0.345 seconds. The last frame thus matches the first frame, except for the appropriate change in particular OM/hook shapes. Most importantly, the final microstructure matches the slab micrograph.

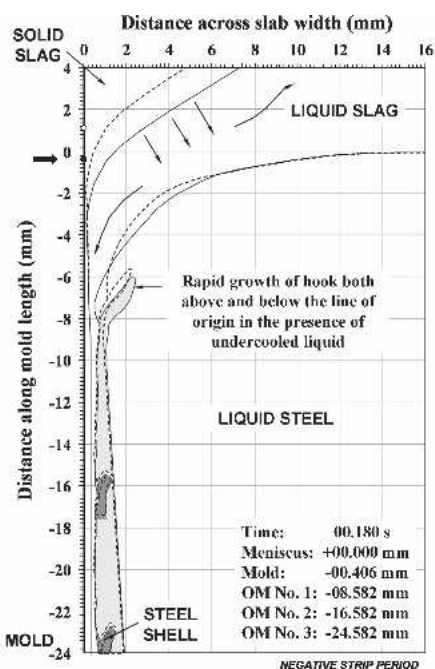
VI. MECHANISM OF HOOK-TYPE OM FORMATION

The process described in Section V, of creating 36 sequential schematics while satisfying many logical constraints, revealed the specific events leading to the formation of



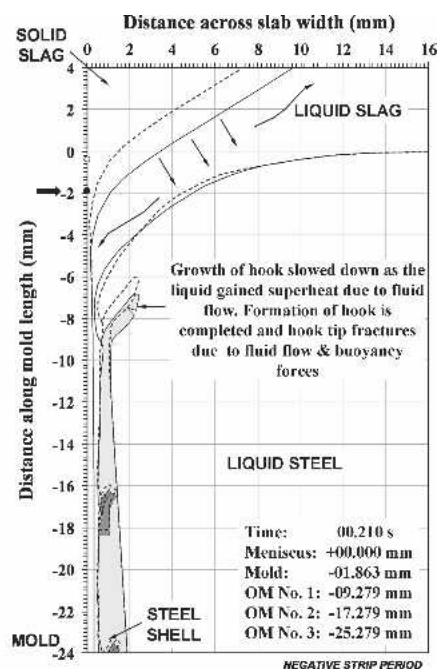
Frame 16 at $t = 0.150$ s
Liquid steel overflow & dendritic growth above line of hook origin begins

(g)



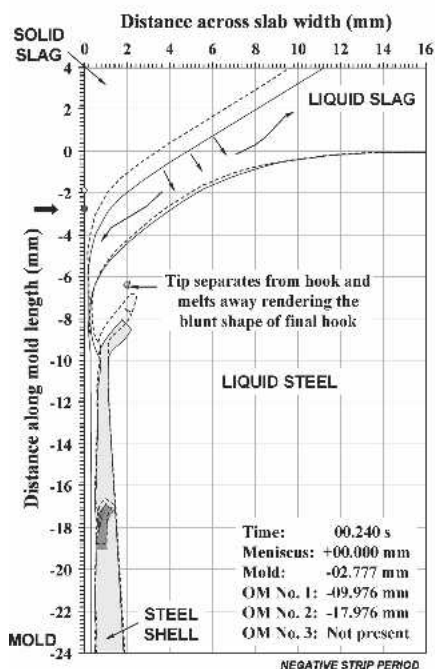
Frame 19 at $t = 0.180$ s
Rapid hook growth

(h)



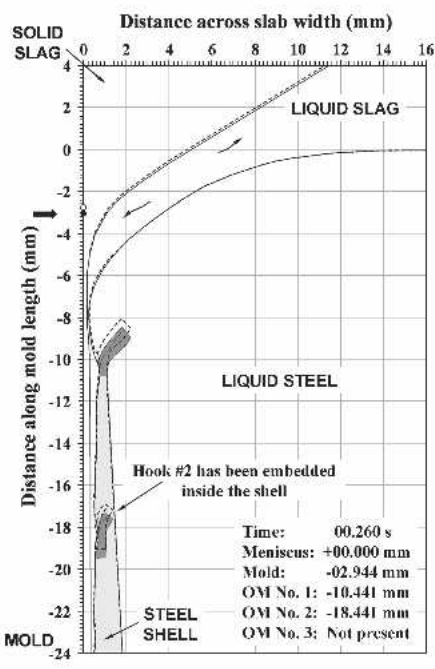
Frame 22 at $t = 0.210$ s
Completion of hook growth followed by hook tip fracture

(i)



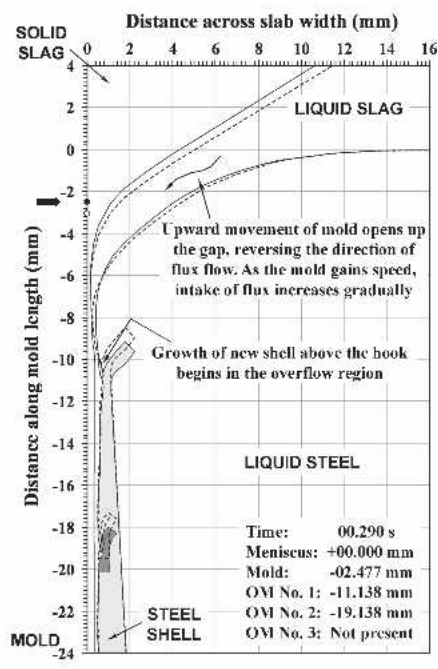
Frame 25 at $t = 0.240$ s
Truncation of hook & end of negative strip

(j)



Frame 27 at $t = 0.260$ s
Lowest position of mold (0.258 s in Figure 9)

(k)



Frame 30 at $t = 0.290$ s
New shell growth

(l)

Fig. 13—(Continued). (a) through (n) Frames depicting events in hook formation, compared with (o) actual slab sample (Table I conditions). Dotted lines indicate positions in the preceding frame.

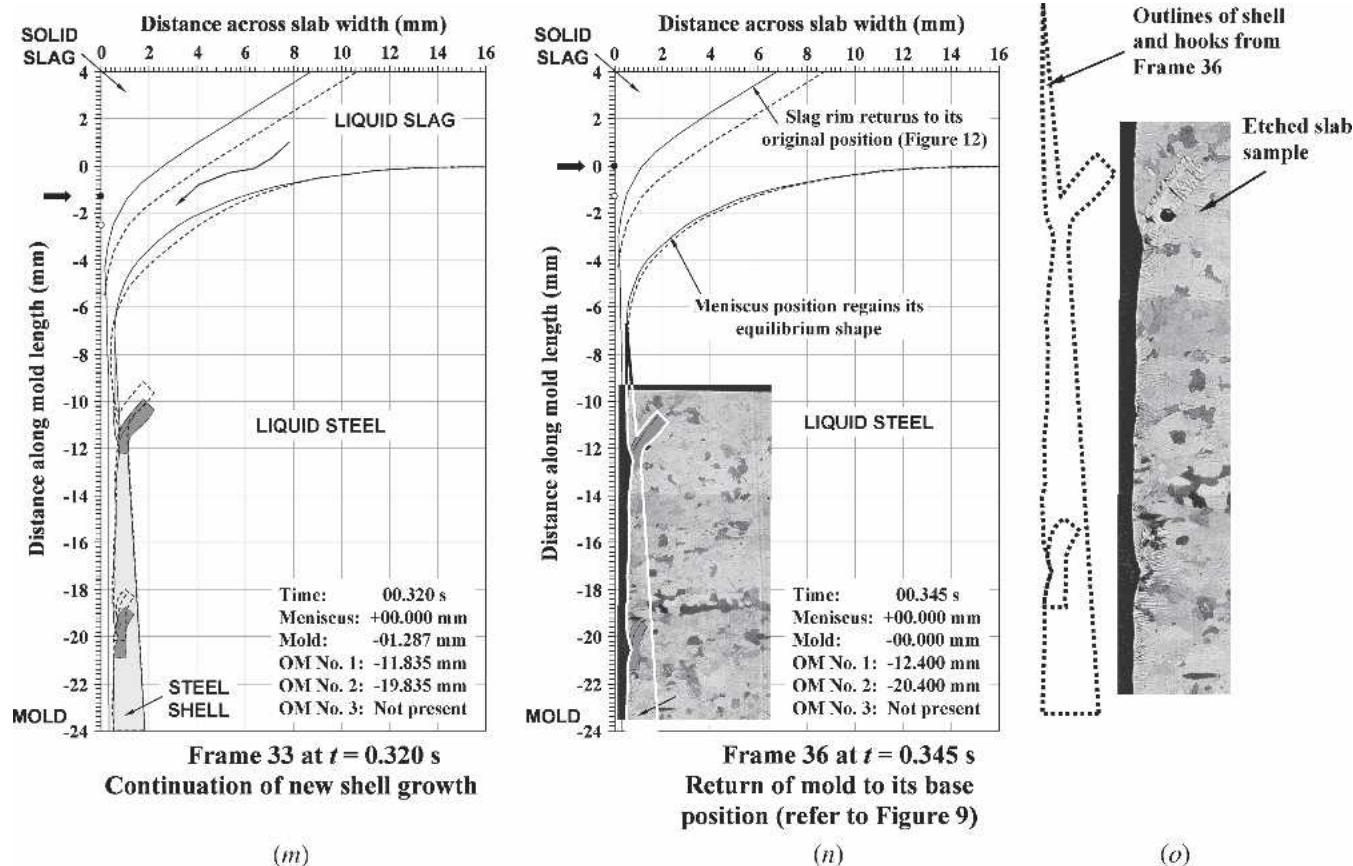


Fig. 13—(Continued). (a) through (n) Frames depicting events in hook formation, compared with (o) actual slab sample (Table I conditions). Dotted lines indicate positions in the preceding frame.

a new hook and OM in ultra-low-carbon steel. Remarkably, a consistent new mechanism was found. For brevity, only frames that depict crucial events are presented in Figures 13(a) through (n) for the times given in Figure 9(b). The animation containing all 36 frames is available elsewhere.^[48]

In Figures 13(a) through (c), the mold moves upward (positive strip time), together with the slag rim. Thus, the gap between the metal level and the solid flux rim gradually opens. This creates negative pressure on the curved meniscus, which causes the meniscus to bulge upward from its equilibrium shape. The negative pressure also draws liquid flux into the gap, thereby increasing mold flux consumption during this time. This suction gradually decreases as flux flows in, mold velocity decreases (Figure 9(a)), and the mold approaches its maximum height of +2.938 mm at ~0.090 seconds (Figure 13(c)).

In Figures 13(d) through (j), the mold moves downward with increasing velocity, overtaking the speed of the solid shell after ~0.110 seconds (Figure 13(d)). This starts the negative strip period. The slag rim moving down with the mold generates positive pressure on the meniscus and pumps liquid flux away, both upward out of the gap and into the channel between the mold and shell. This contributes to some mold flux consumption during this negative strip time and pushes the shell away from the mold. This lubrication effect facilitates smooth withdrawal of the solid shell from the mold, which is why the mold is oscillated.

Several other important events occur during the negative strip time (Figures 13(d) through (j)). The most crucial event is meniscus freezing, which dictates the ultimate shape of the hook. This is clearly evident from Figures 3(b) and (c), which show that the line of hook origin (or shape of frozen meniscus) matches reasonably with Bikerman's equation for the meniscus shape. The hooks are curved much more than the maximum curvature expected from thermal distortion of the initial shell, even for a level fluctuation of 16 mm for 0.4 seconds. Meniscus freezing must occur at ~0.120 seconds (Figure 13(e)), in order to explain the subsequent formation of hook 1. The liquid is undercooled, owing to the high heat transfer in this region combined with the difficulty of nucleation in these steels.^[30] Nucleation and rapid solidification are triggered at this time, perhaps by meniscus movement toward the mold. This event confirms the type III hook mechanism of meniscus freezing.

As the frozen meniscus travels downward with the casting velocity, the liquid meniscus continues to freeze (*i.e.*, dendrites grow from the line of origin into the liquid steel, extending the hook). Until $t = \sim 0.140$ seconds, the meniscus of heavy molten steel supported above the (new) shell tip is precariously balanced by surface tension. However, this situation quickly becomes unstable, and the liquid steel overflows as soon as inertial forces instantaneously exceed surface tension forces, as shown in Figure 13(g). The start of the overflow dictates the maximum possible length of the

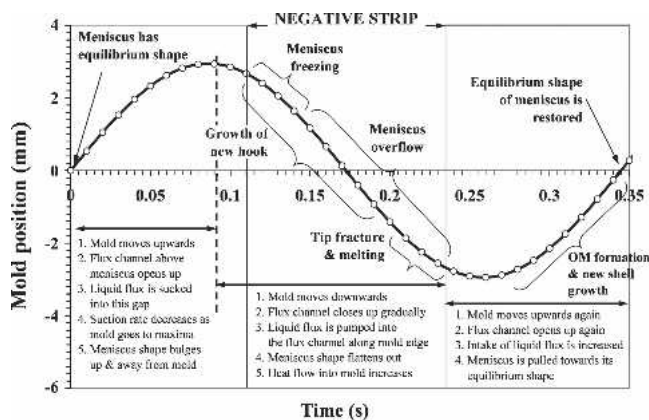


Fig. 14—Summary of steps in formation of a hook-type OM.

hook. For a short time, the colder hook is able to grow rapidly in both directions away from its line of origin. As the hook reheats, solidification naturally slows, allowing interdendritic liquid, mold powder, and other material to concentrate between the gradually coarsening dendrite arms. Very soon, the hook growth stops.

Often, hot tearing breaks off the tip of the fragile hook, as shown in Figure 13(i). Small inertial forces caused by the overflowing liquid steel are likely responsible, because brittle fracture of a semisolid metal needs only ~ 1 pct strain.^[49] The separated hook tip likely floats near the truncated hook and eventually melts away in this case (as in Figures 6(a)). This leads to the truncated hook in Figure 13(j), by the end of negative strip.

The liquid steel overflowing the curved hook surface moves rapidly toward the mold wall during this time of negative strip. This event explains the sharp drop in the distance between the solidified shell and mold wall during the negative strip time measured by Tsutsumi *et al.*^[50] while observing OMs and mold powder infiltration in a Sn-Pb alloy (metal) and stearic acid (flux) system. It also explains the rapid rise of mold heat flux throughout the negative strip time, observed during experiments by Badri *et al.*^[5,28]

The heavier liquid steel displaces liquid mold flux as it overflows. It also melts through some of the solid mold flux layer, bringing liquid steel closer to the mold wall, as shown in Figure 13(j). This explains the eventual outward bulge usually observed above every OM and line of hook origin. For example, in Figure 6(a), the slab surface above the OM extends $d = 0.32$ mm beyond the OM root and 0.16 mm beyond the slab surface below the OM. This indicates that the overflow caused ~ 0.16 mm of the flux layer thickness to remelt. The heat-transfer rate increases during this time because it is controlled by the gradually decreasing thickness of the mold flux layer that separates the mold and the molten steel. The heat-transfer rate is largest while the steel is still liquid, before solidification produces a surface roughness and solid layer that slows heat transfer.

Figure 13(k) shows the instant near the beginning of the positive strip time when the mold is at its lowest position in the oscillation cycle, *i.e.*, ~ -2.944 mm at ~ 0.260 seconds. The direction of flux flow reverses as the gap starts to open and positive pressure is released. As the mold gains upward speed, more flux is drawn into the gap, and mold powder

consumption rises. Additionally, the meniscus is pulled up, approaching the shape predicted by Bikerman. Conventional shell growth next to the mold begins in Figure 13(l) and the OM accompanying hook 1 is created. The volume of flux entrapped in the OM during its formation at this time explains the sudden rise in tracer velocity measured in the stearic acid flux channel between the mold wall and shell^[50] during the positive strip time. Solidification continues in Figures 13(l) and (n), and the complete mold oscillation cycle ends at 0.345 seconds. Figure 13(o) compares a trace of the solid shell in the final frame with the actual shapes obtained from an etched slab sample. The perfect match indicates the accuracy of the schematic.

Frames 1 (Figure 10) and 36 (Figure 13(n)) are the same, except that hooks 1 and 2 in the latter replace hooks 2 and 3 in the former. All of the events described previously will repeat periodically, producing a hook and OM during each mold oscillation cycle. Obviously, chaotic events such as metal level fluctuations may occur at any time during the oscillation cycle and will alter the shapes of OMs and hooks (Figure 5). These events can also create additional OMs/surface depressions (Figure 4(c)) or alter their spacing, by triggering overflow at a different time during the cycle. Each overflow event naturally can create at most one hook. This explains the fact that every single hook observed in over 200 samples of etched hooks was accompanied by an OM.

Oscillation marks are routinely observed without hooks. Hook formation can be avoided in many ways that are consistent with the new mechanism: (1) the meniscus fails to freeze due to high superheat that discourages nucleation; (2) during overflow, most of the hook is melted away, or broken off and carried away; and (3) the hook is detached and transported close to the slab surface, where it cannot be distinguished after etching.

After forming, the hook and its associated OM move down the mold at the casting speed. Hooks 1 and 2 stick out past the solidification front into the liquid. This allows the dendrites in the hook to further coarsen, before the shell eventually catches up and embeds the hooks, and solidification continues past. In addition to this, inclusions and argon bubbles circulating in a liquid steel pool (Figure 2) from near the meniscus to ~ 15 mm below (for this case) can be easily entrapped by these protruding hooks. The OMs align with the maximum heat flux at the meniscus, which agrees with measurements.^[28] Lower down the mold, the OMs align with the local minima in heat flux, owing to their associated thicker mold flux layer and increased gap resistance, as documented previously.^[4,51]

The events in Figures 13(a) through (n) are summarized in Figure 14. This new hook formation mechanism contrasts with the two main previous theories as follows.

- (1) The type II mechanism, where hooks form by shell bending, is contradicted. It seems unlikely that mechanical forces could be large enough to bend the steel into the exact shape of a frozen meniscus without breaking it.
- (2) The type III mechanism, where hooks form by meniscus solidification, is generally supported. However, the new mechanism proposes that liquid steel overflow occurs during negative strip, causing a rapid increase of mold heat flux. This contradicts almost all previous

mechanisms, but it is supported by the recent experimental findings by Badri *et al.* and Tsutsumi *et al.*

- (3) The new mechanism explains details of the hook microstructure, such as the dendrite structure spreading both ways from the line of hook origin, truncation of the hook tip, and the OM associated with each hook. No previous mechanism has done this.

VII. VERIFICATION OF THE NEW HOOK MECHANISM

This section validates the proposed new mechanism of hook formation by systematically explaining each of the trends observed in the industrial trials in Section IV.^[9,10]

- (1) *Powder consumption rate increases strongly during positive strip time:* Liquid flux is drawn into the gap between the solid flux rim and the meniscus as it opens due to the upward movement of the mold.
- (2) *Powder consumption rate increases during negative strip time:* More liquid flux is squeezed into the channel between the shell and mold due to the positive pressure generated by the downward motion of the solid flux rim during this time.
- (3) *Mean depth of hook increases with increase in negative strip time:* A longer negative strip time prolongs meniscus freezing time before overflow, allowing more of the meniscus to freeze, producing a longer, deeper hook.
- (4) *Mean depth of hook decreases with increasing casting speed:* Increasing the casting speed increases the local superheat at the solidification front^[44] so discouraging meniscus freezing. Also, the shell moving downward faster will trigger overflow sooner. Both effects produce less-frequent and shallower hooks.
- (5) *Mean hook shell thickness decreases with increasing casting speed:* Less time is available for the hook to grow below and above the line of origin, so thinner hooks are created.
- (6) *Mean depth of hook decreases with increasing oscillation frequency:* Less time is available before liquid overflow as the negative strip time is shortened, so hooks will be shorter.
- (7) *Mean hook shell thickness decreases with increasing oscillation frequency:* Less time is available for meniscus freezing as the negative strip time is shortened, so hooks will be thinner.
- (8) *Mean length of hook decreases with increasing tundish temperature:* Increased superheat retards meniscus freezing. After liquid steel overflow, it slows hook growth and encourages melting.
- (9) *Mean depth of hook increases with increasing thickness of hook shell:* Increased hook shell thickness indicates either more time for hook growth or more undercooling during overflow. Either case promotes meniscus freezing, so the hook length is increased.

VIII. SUMMARY AND CONCLUSIONS

Subsurface hooks and OMs form in continuously cast steel slabs through a complex mechanism involving many interdependent, transient thermal-fluid flow phenomena that occur during initial solidification near the meniscus.

This article presents a series of schematics to reveal the details of this mechanism in ultra-low-carbon steel. They were constructed from careful analysis of hook features observed on numerous specially etched samples obtained from an industrial caster combined with previous experimental observations and theoretical modeling results. The steps in the mechanism are summarized as follows.

- (1) At the start of the negative strip time, the undercooled meniscus suddenly solidifies. The shape of the meniscus at this instant dictates the curvature of the line of hook origin.
- (2) Next, dendrites quickly grow into undercooled liquid steel from nucleation sites on the frozen meniscus, creating the hook shell thickness below the line of hook origin.
- (3) As the shell tip moves downward, the meniscus supported above the hook becomes unstable and overflows. This usually occurs near the start of negative strip, increasing heat flux to the mold during the negative strip time. Level fluctuations may initiate this overflow event at other times, however, resulting in pitch variations.
- (4) Dendrites quickly solidify into the undercooled overflowed liquid from the line of hook origin toward the mold wall. Growth soon stops as the meniscus region reheats, coarsening the dendrites and distinguishing the hook edges.
- (5) Final shape of the hook is completed as the hook tip fractures and melts away.
- (6) The remaining overflowed, supercooled liquid solidifies. Until this happens, the extent of the liquid penetration into filling the gap and remelting the interfacial flux layer determines the final shape of the upper side of the OM. Any debris trapped within the overflowed liquid creates surface defects.
- (7) The hook protruding from the solidifying shell further captures inclusions and bubbles rising up the solidification until the shell finally solidifies past the hook.

The match between measured hook shapes and Bikerman's equation provides evidence for meniscus freezing. Meniscus overflow during the negative strip time is justified by two independent experimental observations in prior work: (1) periodic rise in heat flux into the mold during negative strip and (2) a sharp drop in the distance between the solidified shell and mold wall during negative strip. The new mechanism also explains several correlations between hook characteristics and casting variables observed in plant experiments.

The novel stepwise graphical approach of this work, simultaneously satisfying separate pieces of knowledge from several different sources, enabled the development of this robust new mechanism. This will provide a foundation for future computational models to quantify hook and OM formation in other grades and conditions. This new fundamental understanding will ultimately lead to optimized practices to minimize these surface defects during continuous casting.

ACKNOWLEDGMENTS

The authors thank the Natural Sciences and Engineering Research Council of Canada, the National Science

Foundation (Grant No. DMI-05-28668), and the Continuous Casting Consortium, the University of Illinois at Urbana-Champaign, for support of this project. The technical support extended by POSCO personnel, J.M. Park, C.H. Lee, W.Y. Choi, and J.H. Park, is gratefully acknowledged.

REFERENCES

1. E. Takeuchi and J.K. Brimacombe: *Metall. Trans. B*, 1984, vol. 15B, pp. 493-509.
2. T. Emi, H. Nakato, Y. Iida, K. Emoto, R. Tachibana, T. Imai, and H. Bada: *Proc. Nat. Open Hearth and Basic Oxygen Steel Conf.*, 1978, vol. 61, pp. 350-61.
3. S.N. Singh and K.E. Blazek: *J. Met.*, 1974, vol. 26 (10), pp. 17-23.
4. M.S. Jenkins, B.G. Thomas, W.C. Chen, and R.B. Mahapatra: *Proc. 77th Steelmaking Conf.*, Chicago, IL, 1994, ISS, Warrendale, PA, 1994, pp. 337-45.
5. A. Badri, T.T. Natarajan, C.C. Snyder, K.D. Powers, F.J. Mannion, and A. Cramb: *Metall. Mater. Trans. B*, 2005, vol. 36B, pp. 355-71.
6. K. Schwerdtfeger and H. Sha: *Metall. Mater. Trans. B*, 2000, vol. 31B, pp. 813-26.
7. M. Suzuki: *CAMP-ISIJ*, 1998, vol. 11, pp. 42-44.
8. E. Takeuchi and J.K. Brimacombe: *Metall. Trans. B*, 1985, vol. 16B, pp. 605-25.
9. H.-J. Shin, G.-G. Lee, W.-Y. Choi, S.-M. Kang, J.-H. Park, S.-H. Kim, and B.G. Thomas: *MS&T 2004 Conf. Proc.*, New Orleans, LA, 2004, The Association for Iron and Steel Technology (AIST) and TMS, Warrendale, PA, 2004, pp. 11-26.
10. H.-J. Shin, G.-G. Lee, W.-Y. Choi, S.-M. Kang, J.-H. Park, S.-H. Kim, and B.G. Thomas: *AISTech 2004 Iron and Steel Technology Conf. Proc.-Vol. II*, Nashville, TN, 2004, The Association for Iron and Steel Technology (AIST), Warrendale, PA, 2004, pp. 1157-70.
11. C. Genzano, J. Madias, D. Dalmaso, J. Petroni, D. Biurrun, and G.D. Gresia: *Iron Steelmaker*, 2002, vol. 29 (6), pp. 23-26.
12. K. Bo, G. Cheng, J. Wu, P. Zhao, and J. Wang: *J. Univ. Sci. Technol. Beijing*, 2000, vol. 7 (3), pp. 189-92.
13. K.D. Schmidt, F. Friedel, K. Imlau, W. Jager, and K.T. Muller: *Steel Res. Int.*, 2003, vol. 74 (11-12), pp. 659-66.
14. J.-P. Birat, M. Larrecq, J.-Y. Lamant, and J. Petegnief: *Steelmaking Conf. Proc.*, 1991, vol. 74, pp. 39-40.
15. J.K. Brimacombe and K. Sorimachi: *Metall. Trans. B*, 1977, vol. 8B, pp. 489-505.
16. S. Harada, S. Tanaka, H. Misumi, S. Mizoguchi, and J. Horiguchi: *Iron Steel Inst. Jpn. Int.*, 1990, vol. 30 (4), pp. 310-16.
17. H. Fredriksson and J. Elfsberg: *Scand. J. Metall.*, 2002, vol. 31, pp. 292-97.
18. I.G. Saucedo: *Steelmaking Conf. Proc.*, Warrendale, PA, 1991, ISS-AIME, Warrendale, PA, 1991, pp. 43-53.
19. M.M. Wolf: *PTD Conf. Proc.*, Nashville, TN, ISS, Warrendale, PA, 1995, pp. 99-117.
20. Y. Kitano: *Tetsu-to-Hagane*, 1994, vol. 80, pp. T165-68.
21. Y. Meng and B.G. Thomas: *Metall. Trans. B*, 2003, vol. 34B, pp. 685-705.
22. K. Miyazawa and T. Mizoguchi: *Japan Cooperative Science Program Seminar on Solidification Processing of Advanced Materials*, Kanagawa, Japan, Japan Society for Promotion of Science Tokyo, Japan, and National Science Foundation, Arlington, VA, 1989, pp. 235-44.
23. S. Takeuchi, Y. Miki, S. Itoyama, K. Kobayashi, K. Sorimachi, and T. Sakuraya: *Steelmaking Conf. Proc.*, 1991, pp. 37-41.
24. T. Tanaka and K. Takatani: *CAMP-ISIJ*, 1989, vol. 2, p. 1263.
25. R.S. Laki, J. Beech, and G.J. Davies: *Ironmaking and Steelmaking*, 1984, vol. 11 (5), pp. 283-91.
26. B.G. Thomas: *Metall. Mater. Trans. B*, 2002, vol. 33B, pp. 795-812.
27. Y. Meng and B.G. Thomas: *Metall. Mater. Trans. B*, 2003, vol. 34B, pp. 707-25.
28. A. Badri, T.T. Natarajan, C.C. Snyder, K.D. Powers, F.J. Mannion, M. Byrne, and A. Cramb: *Metall. Mater. Trans. B*, 2005, vol. 36B, pp. 373-83.
29. H. Yamamura, Y. Mizukami, and K. Misawa: *Iron Steel Inst. Jpn. Int. (Suppl.)*, 1996, vol. 36, pp. S223-26.
30. H. Mizukami, S. Hiraki, M. Kawamoto, and T. Watanabe: *Iron Steel Inst. Jpn. Int.*, 1999, vol. 39 (12), pp. 1261-69.
31. B.G. Thomas and H. Zhu: *Proc. JIM/TMS Solidification Science and Processing Conf.*, Honolulu, HI, 1995, TMS, Warrendale, PA, 1995, pp. 197-208.
32. E.S. Szekeres: *Iron Steel Eng.*, 1996, vol. 73 (7), pp. 29-37.
33. F. Yigit, L.G. Hector, and O. Richmond: *J. Thermal Stresses*, 2002, vol. 25 (8), pp. 773-809.
34. R. Hentrich, D.L. Sharma, D. Dittert, and E. Roller: *Iron Steelmaker*, 1986, vol. 13 (4), pp. 34-41.
35. R. Sato: *Proc. National Open Hearth and Basic Oxygen Steel Conf.*, Detroit, MI, 1979, AIME, Warrendale, PA, 1979, pp. 48-67.
36. J. Savage and W.H. Pritchard: *Iron Steel*, 1954, vol. 27 (14), pp. 649-52.
37. C. Bernhard, H. Hiebler, and M.M. Wolf: *Ironmaking and Steelmaking*, 2000, vol. 27 (6), pp. 450-54.
38. S. Itoyama, H. Yamanaka, S. Tanaka, T. Yunde, and T. Kuroki: *ISS Steelmaking Conf. Proc.*, 1988, vol. 71, pp. 97-102.
39. A.W. Cramb and F.J. Mannion: *Steelmaking Conf. Proc.*, 1985, vol. pp. 349-59.
40. J. Sengupta and B.G. Thomas: *Continuous Casting Consortium Annual Report 2005: Mathematical Models of Continuous Casting of Steel*, University of Illinois, Urbana, IL, 2005, vol. IL, pp. 1-99.
41. W. Lai, M. Milone, and I.V. Samarasekera: *83rd Steelmaking Conf. Proc.*, ISS-AIME, Warrendale, PA, 2000, pp. 261-74.
42. O. Putz, O. Breinfeld, and S. Rodl: *Steel Res.*, 2003, vol. 74 (11-12), pp. 686-92.
43. O. Putz and S. Rodl: *Steel Res.*, 2003, vol. 74 (2), pp. 104-13.
44. X. Huang and B.G. Thomas: *Can. Metall. Q.*, 1998, vol. 37 (3-4), pp. 197-212.
45. I. Jimbo and A.W. Cramb: *Iron Steelmaker*, 1993, vol. 20 (6), pp. 55-63.
46. J. Lee and K. Morita: *Iron Steel Inst. Jpn. Int.*, 2002, vol. 42 (6), pp. 588-94.
47. S. Furuhashi, M. Yoshida, and T. Tanaka: *Tetsu-to-Hagane*, 1998, vol. 84 (9), pp. 625-31.
48. J. Sengupta and B.G. Thomas: *JOM-e, Electronic Supplement to J. Mater. (JOM)*, TMS, unpublished research, 2006.
49. H. Mizukami, A. Yamanaka, and T. Watanabe: *Iron Steel Inst. Jpn. Int.*, 2002, vol. 42 (9), pp. 964-73.
50. K. Tsutsumi, J. Ohtake, and M. Hino: *Iron Steel Inst. Jpn. Int.*, 2000, vol. 40, pp. 601-08.
51. D.T. Lui: Master's Thesis, University of Illinois at Urbana-Champaign, Urbana, IL, 1995.